AIAA JOURNAL
Vol. 32, No. 11, November 1994

Buckling of Elastoplastic Circular Cylindrical Shells Under Axial Compression

M. C. Lin* and M. K. Yeh†
National Tsing Hua University, Hsinchu, Taiwan 30043, Republic of China

The buckling behavior of elastoplastic circular cylindrical shells under axial compression was investigated analytically and experimentally. For analysis, a finite element code based on the updated Lagrangian formulation was established to analyze the axial buckling problem by considering nonlinear geometric and material properties. An iterative displacement-controlled scheme was adopted in the solution procedure to avoid numerical instability near the buckling load. The ratios of diameter to thickness considered were between 25 and 400. A compressive testing machine was used to perform the axial buckling experiments. The ratios of diameter to thickness of the aluminum specimens were 100 and 133. It was found that the buckling strength was reduced by variations of initial thickness along the axis of the cylindrical shell. The ratio of length to diameter and the boundary conditions had little influence on the buckling loads, but caused varied postbuckling behavior.

Introduction

CIRCULAR cylindrical shells are commonly used in engineering structures, such as planes, missiles, silos, and tanks. During their service life, these structures are subjected to loadings of various types. In past investigations of the stability of elastic isotropic cylindrical shells under axial compression, Ramsey[1] examined elastic axisymmetric axial buckling of infinitely long shells using the Cosserat surface theory. The elastic buckling analyses of glass-reinforced plastic cylindrical shells using finite element code NONL5 were reported by Abu-Farsakh and Lusher[2] and Abu-Farsakh.[3]

When compared with results predicted by linearized, elastic, small deflection theories, previous work showed that the experimental results were much smaller than analytical buckling loads due to the influence of imperfections. Hansen[4] investigated the effect of random imperfections on the elastic buckling of circular cylindrical shells. Liu and Li[5] used a stress hybrid shallow shell element to examine the influences of initial ovality and lack of straightness on the elastic buckling stress of cylindrical shells. The imperfection sensitivity of elastic axial buckling was adopted to solve some other related problems. For instance, Rotter and Teng[6] and Rotter and Zhang[7] treated the welded joints on circular cylindrical shells as imperfections to determine their axial buckling strengths. Krishnakumar and Foster[8,9] and Foster[10] studied the influence of imposed diamond local dimples on the buckling loads of isotropic epoxy shells experimentally.

For metals, buckling of cylindrical shells with relatively small diameter-to-thickness ratios usually occurs in the plastic range. Axial buckling of cylindrical shells compressed into the plastic range was investigated as early as 1949 by Bijlaard.[11] Lee[12] and Batterman[13] showed that relatively thick cylindrical shells under axial compression buckled with an axisymmetric mode. Sobel and Newman[14] examined the elastoplastic buckling of circular cylindrical steel shells with a ratio of diameter to thickness of about 37 experimentally and analytically. The effect of initial geometric imperfections on the plastic buckling of axially compressed cylindrical shells was also studied.[15–20] Batterman and Lee[15] found that the effect of initial imperfections was enormous for the diamond-shaped circumferential mode buckling according to incremental theory. Gellin[17] investigated shells with a sinusoidal axisymmetric imperfection based on the J_2 deformation theory. Yun and Kyriakides[18] assessed the so-called "beam" and "shell" modes of buckling of buried pipelines under axially compressive loads; they demonstrated that initial geometric imperfections could strongly influence the critical loads and strains for both types of instability. Tvergaard[19,20] analyzed the problem of elastic-plastic cylindrical shells with initial axisymmetric imperfection that bifurcated into a nonaxisymmetric shape; his analysis includes the possibility of localization of buckling modes. Ramsey[21] treated the material as rigid plastic with isotropic work hardening and found that the localization of axial buckling deformation was governed by the ratio of radius to thickness of the cylindrical shells.

Since imperfections reduce the axial buckling strength of elastic circular cylindrical shells, we present a way to investigate the effect of initial imperfections on the buckling strength of elastoplastic circular cylindrical shells. Elastoplastic material behavior was considered, and a finite element code based on the updated Lagrangian formulation[22,23] was developed to analyze elastoplastic buckling and postbuckling behavior of circular cylindrical shells under axial compression. An incremental displacement-controlled scheme was adopted to avoid divergence near the buckling load. The analytical results are compared with experimental ones for aluminum circular cylindrical shells with ratios of diameter to thickness of 100 and 133. The axial buckling loads of elastoplastic circular cylindrical shells are shown for ratios of diameter to thickness in the range 25–400. The effect of different boundary conditions on the elastoplastic buckling and postbuckling behavior is also presented.

Updated Lagrangian Formulation

As the shell surface undergoes large displacements and large rotations for the buckling problem, the updated Lagrangian formula-

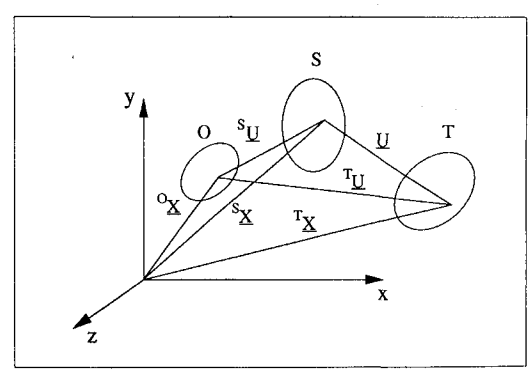

Fig. 1 Motion of body in a stationary Cartesian system.

Received Nov. 27, 1993; revision received May 16, 1994; accepted for publication May 20, 1994.

*Graduate Student, Department of Power Mechanical Engineering.
†Associate Professor, Department of Power Mechanical Engineering. Member AIAA.

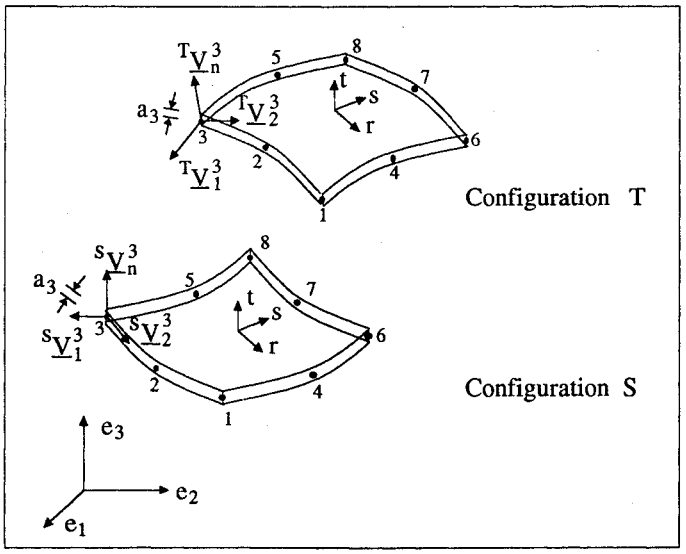

Fig. 2 Shell element undergoing large displacements and rotations.

tion was adopted to treat this nonlinear geometry problem. As shown in Fig. 1, the body moves and deforms from the original configuration O to the current configuration S; all variables and the equilibrium of the body in the current configuration S are known and used to obtain the next required equilibrium configuration T. The linearized equilibrium equation of the problem was derived from the principle of virtual work[22] as

$$\int_V C_{ijrs} e_{rs} \delta e_{ij}\, dV + \int_V \tau_{ij} \delta \eta_{ij}\, dV = \int_{T_A} {}^T P_i \delta u_i\, dA - \int_V \tau_{ij} \delta e_{ij}\, dV \tag{1}$$

in which C_{ijrs} is the elasticity tensor, e_{ij} and η_{ij} are the linear and the nonlinear parts of the strain increment tensor, τ_{ij} is the Cauchy stress tensor, and u_i is the corresponding displacement at the point where the external force ${}^T P_i$ is applied. All of these tensors were considered in the current configuration S, whereas the external force ${}^T P_i$ was referred to the next required configuration T.

Finite Element Method

The degenerated shell element[24] with eight nodal points was used to discretize the continuous system. This element geometry was interpolated using the midsurface nodal point coordinates and midsurface nodal point normals. It is assumed that lines that were originally normal to the midsurface of the shell remained straight during the element deformation and that no transverse normal stress was developed. As shown in Fig. 2, (r, s, t) is a set of orthogonal natural coordinates for the element. The coordinates of a generic point in the shell element undergoing large displacements and rotations were interpolated as

$$\boldsymbol{X} = \sum_{k=1}^{8} N_k \boldsymbol{X}^k + \frac{\zeta}{2} \sum_{k=1}^{8} a_k N_k \boldsymbol{V}^k \tag{2}$$

in which $N_k = N_k(r, s, t)$ is the shape function at nodal point k, $\boldsymbol{X}^k$ is the local coordinate of nodal point k, ζ is the local coordinate in the thickness direction, a_k is the thickness at the nodal point k, and $\boldsymbol{V}^k$ is the unit normal vector to the midsurface at nodal point k.

The incremental displacement $\boldsymbol{U}_e$ of a generic point in this element from configuration S to configuration T is expressed as

$$\boldsymbol{U}_e = \sum_{k=1}^{8} N_k \boldsymbol{U}^k + \frac{\zeta}{2} \sum_{k=1}^{8} a_k N_k \left(-\boldsymbol{V}_2^k \alpha_k + \boldsymbol{V}_1^k \beta_k \right) \tag{3}$$

in which $\boldsymbol{U}^k = \left(u_r^k, u_s^k, u_t^k \right)$ is the incremental displacement at nodal point k; α_k and β_k are rotations along the directions $\boldsymbol{V}_1^k$ and $\boldsymbol{V}_2^k$, which form a set of orthogonal vectors with $\boldsymbol{V}^k$, as shown in Fig. 2. There are five degrees of freedom—u_r^k, u_s^k, u_t^k, α_k, and β_k—for each nodal point. With the coordinate transformation between the local coordinates (r, s, t) and the global Cartesian coordinates (x, y, z), the equilibrium equation (1) can be expressed in the following form in global coordinates for each element as

$$\{ [K]_l + [K]_{nl} \} \boldsymbol{U}_e = {}^T \boldsymbol{P}_e - \boldsymbol{F}_e \tag{4}$$

where

$$[K]_l = \int_V [B]_L^T [C]\, [B]_L\, dV \tag{5}$$

$$[K]_{nl} = \int_V [B]_{NL}^T [\tau]\, [B]_{NL}\, dV \tag{6}$$

$${}^T \boldsymbol{P}_e = \int_{T_A} {}^T \boldsymbol{P}_i \delta u_i\, dA \tag{7}$$

$$\boldsymbol{F}_e = \int_V [B]_L^T \tau\, dV \tag{8}$$

In Eqs. (4–8), $[K]_l$ and $[K]_{nl}$ are the linear and nonlinear parts of the element stiffness matrices, $[B]_L$ and $[B]_{NL}$ are the corresponding linear and nonlinear strain-displacement transformation matrices, $[C]$ is the material property matrix, $[\tau]$ and τ are the Cauchy stress matrix and stress vector, ${}^T \boldsymbol{P}_e$ is the effective force vector in the configuration T, and $\boldsymbol{F}_e$ is the internal nodal point force vector.

Assembling the element equilibrium equation, Eq. (4), we express the global system equilibrium equation as

$$\{ [K]_L + [K]_{NL} \} \boldsymbol{U} = {}^T \boldsymbol{P} - \boldsymbol{F} \tag{9}$$

in which $[K]_L$ and $[K]_{NL}$ are the linear and nonlinear parts of the global stiffness matix, $\boldsymbol{U}$ is the global displacement incremental vector from the current configuration S to the next required configuration T, ${}^T \boldsymbol{P}$ is the global effective applied force vector in the configuration T, and $\boldsymbol{F}$ is the internal force vector in the configuration S.

Elastoplastic Materials

For hardening materials, the Ramberg-Osgood equation was used to fit the uniaxial stress-strain curve:

$$\varepsilon = \frac{\sigma}{E} + \frac{3}{7} \frac{\sigma}{E} \left(\frac{\sigma}{\sigma_y} \right)^{n-1} \tag{10}$$

in which ε and σ are the axial strain and stress, E is the elastic Young's modulus, σ_y is the yield parameter, and n is the hardening parameter.

If the material remains elastic, the elastic material property matrix $[C_e]$ under the assumption that the stress in the shell normal direction remains zero is

$$[C_e] = \frac{E}{(1-\nu^2)} \begin{bmatrix} 1 & \nu & 0 & 0 & 0 & 0 \\ \nu & 1 & 0 & 0 & 0 & 0 \\ 0 & 0 & 0 & 0 & 0 & 0 \\ 0 & 0 & 0 & \dfrac{1-\nu}{2} & 0 & 0 \\ 0 & 0 & 0 & 0 & \dfrac{1-\nu}{2(1.2)} & 0 \\ 0 & 0 & 0 & 0 & 0 & \dfrac{1-\nu}{2(1.2)} \end{bmatrix} \tag{11}$$

in which ν is Poisson's ratio. The factor 1.2 is included in the matrix to correct the uniform shear stress assumption through the

thickness direction.[25] If the material is loaded beyond the yielding surface, the elastoplastic material property matrix $[C_{ep}]$ must be used:

$$[C_{ep}] = [C_e] - \frac{[C_e]\{a\}(\{a\}^T[C_e])}{H + \{a\}^T[C_e]\{a\}} \tag{12}$$

in which

$$\{a\} = \frac{\partial F(\underline{\sigma})}{\partial \underline{\sigma}} \tag{13}$$

$$H = \frac{7}{3}\frac{E}{n}\left(\frac{\sigma_y}{\sigma}\right)^{n-1} \tag{14}$$

For plastic material behavior, we assumed that under the multiaxial stress state the effective stress-strain relation was equivalent to the uniaxial stress-strain relation. The isotropic hardening rule was used for further yielding of the material based on the J_2 flow theory,

$$F(\underline{\sigma}) = \sqrt{3J_2} - \sigma_{\max} = 0 \tag{15}$$

in which $\sqrt{3J_2}$ is the effective stress, and $\sigma_{\max}$ represents the greatest value that $\underline{\sigma}$ reached in the loading history. The initial value of $\sigma_{\max}$ used in the analysis was $0.6\sigma_y$. Equation (15) was used to judge whether further loading occurs for each Gaussian integration point in the process of forming the stiffness matrix.

Displacement-Controlled Incremental Procedure

In solving the system equilibrium equation, Eq. (9), the equation is expressed in the iterative form[22,23] as

$$\{[K]_L + [K]_{NL}\}\boldsymbol{U}^{(i)} = {}^T\boldsymbol{P}^{(i)} - {}^T\boldsymbol{F}^{(i-1)} \tag{16}$$

in which i represents the iteration index. In Eq. (16), $[K]_L$ and $[K]_{NL}$ were not updated in an incremental step, and ${}^T\boldsymbol{F}^{(i-1)}$ was calculated based on the prior state $i-1$.

A displacement-controlled scheme was used to avoid numerical instability near the buckling load. The end displacements of the circular cylindrical shells were used as the controlling increment. The shells had no external forces applied except on the two ends. In each increment, the known end controlling displacements were eliminated from the displacement vector $\boldsymbol{U}^{(i)}$ with proper modifications made to the stiffness matrix and external force vector. Then the condensed form of the equilibrium equation is

$$\{[K]_{LC} + [K]_{NLC}\}\boldsymbol{U}_C^{(i)} = {}^T\boldsymbol{P}_C^{(i)} - {}^T\boldsymbol{F}_C^{(i-1)} \tag{17}$$

in which subscript C means "condensed." Thus, all entries of $\boldsymbol{U}_C^{(i)}$ are unknown, and all entries of ${}^T\boldsymbol{P}_C^{(i)}$ and ${}^T\boldsymbol{F}_C^{(i-1)}$ are known; $\boldsymbol{U}_C^{(i)}$ was solved easily, and ${}^T\boldsymbol{P}^{(i)}$ in Eq. (16) was calculated thereafter. As Eq. (17) is of the iterative type, the iterative process stopped only when the following convergence criterion based on the displacement was satisfied:

$$\frac{\|\boldsymbol{U}_C^{(i)}\|}{\left\|\sum_i \boldsymbol{U}^{(i)}\right\|} < \varepsilon_D \tag{18}$$

in which ε_D is a chosen convergence tolerance, 0.001. The total displacement vector ${}^T\boldsymbol{U}$ in the required configuration T was obtained:

$${}^T\boldsymbol{U} = {}^S\boldsymbol{U} + \sum_i \boldsymbol{U}^{(i)} \tag{19}$$

in which ${}^S\boldsymbol{U}$ is the displacement vector in the current configuration S.

Experiment

A testing machine was used to perform the axial buckling experiments on the circular cylindrical shells. A load cell and one displacement transducer were used to measure the compressive force and the axial displacement of the tested shells, respectively. The signals of the load cell and the displacement transducer were amplified and collected by a data acquisition card built into a microcomputer.

The specimens used in the buckling experiment were made of aluminum alloy 6061-T6. The ratios of nominal diameter to thickness of the specimens were 100 and 133, and the lengths were 97 and 190 mm; the inside diameter was 96 mm. To simulate the fixed-end boundary condition, we used a clamping set to fix the ends of the specimens with epoxy.

Six strip specimens were cut from the circular cylindrical shells to find the material parameters. Equation (10) was used to fit these testing stress-strain curves. The average material parameters obtained are $E = 66.9$ GPa, $\sigma_y = 240$ MPa, $n = 28.8$, and $\nu = 0.34$. The 0.2% offset yield stress σ_0 is also calculated to be 242 MPa. All of these parameters were used in the numerical analysis.

Results and Discussion

The well-known elastic axial buckling stress σ_{cr} of a cylindrical shell is

$$\sigma_{cr} = \frac{2Et}{D\sqrt{3(1-\nu^2)}} \tag{20}$$

in which D and t are, respectively, the diameter and thickness of the circular cylindrical shell. A necessary condition for the use of Eq. (20) is that $\sigma_{cr} < \sigma_0$, the yield stress of the shell. If σ_{cr} calculated is larger than σ_0, the inelastic behavior affects buckling and must be considered.

The analytical load-displacement responses of elastoplastic circular cylindrical shells ($D/t = 100$, $L/D = 1$, $D = 97$ mm) under axial compression are shown in Fig. 3 in which the axial load P and axial shortening u_y were made dimensionless by $P_y = \pi Dt\sigma_0$ and the length of shell L, respectively. The Ramberg-Osgood material behavior, obtained by multiplying the axial stress in the shell with its end cross-section area πDt, is also shown in this figure for an idealized nonbuckling circular cylindrical shell. According to Fig. 3, the postbuckling response of the elastoplastic buckling curve is distinct from the nonbuckling one.

Typical analytical and experimental curves are shown in Fig. 4 for shells with $D/t = 100$, $L/D = 1.96$, and $D = 97$ mm. The limit load type of buckling is considered. The experimental buckling

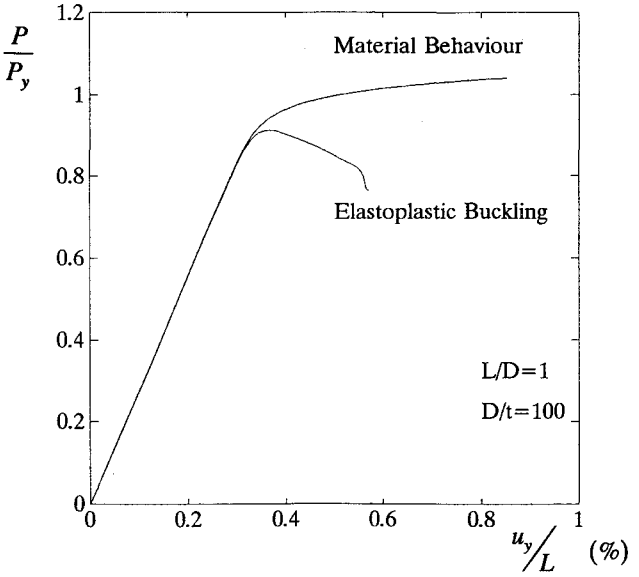

Fig. 3 Load-displacement responses of circular cylindrical shells under axial compression.

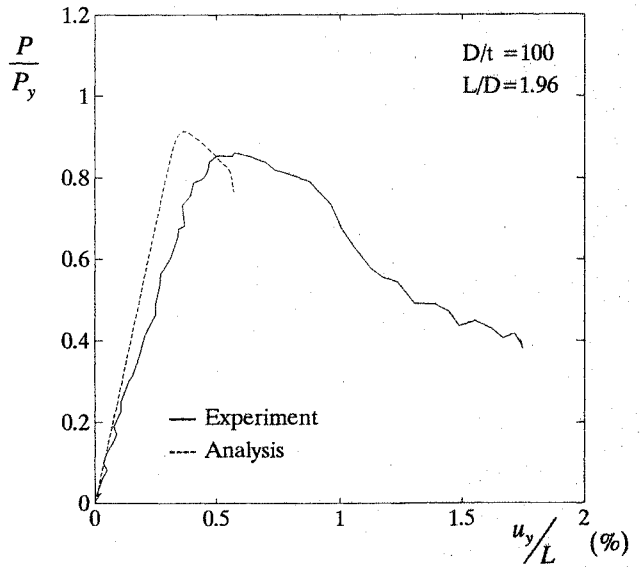

Fig. 4 Analytical and experimental responses of circular cylindrical shells under axial compression.

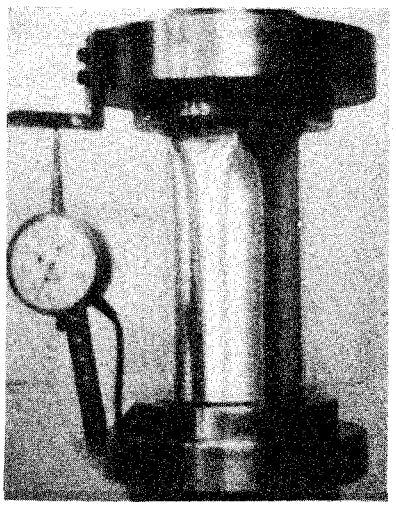

Fig. 5 Experimental buckling deformation of circular cylindrical shells under axial compression.

load is about 3% lower than the analytical one. A bulged ring combined with four semi-diamond-shaped indentations suddenly appeared at the limit load (Fig. 5). As the experiment continued, the axial load kept decreasing as shown in Fig. 4, and the deformation became severe. The ring-type deformation was also observed by Lee,[12] Batterman,[13] and Sobel and Newman[14] for thick shells, and the diamond shape resulted from the buckling of thin shells. The clamped ends made the bulged ring occur easily near one end. As the specimens were relatively thin, thin shells adapted the diamond shape.

The analytical load-displacement responses of circular cylindrical shells under axial compression with different boundary conditions are shown in Fig. 6. The boundary conditions considered here are simply supported ends, one end simply supported and the other clamped, and clamped ends. The axial buckling loads for these three boundary conditions were similar, whereas the post-buckling behavior varied, as shown in Fig. 6. The deformed shapes at buckling of circular cylindrical shells with both ends simply supported and both ends clamped are, respectively, shown in Fig. 7. The deformed shape with simply supported ends, shown in Fig. 7a, consisted of diamond-shaped indentations near the ends, but the one with clamped ends (Fig. 7b) consisted of ring shapes.

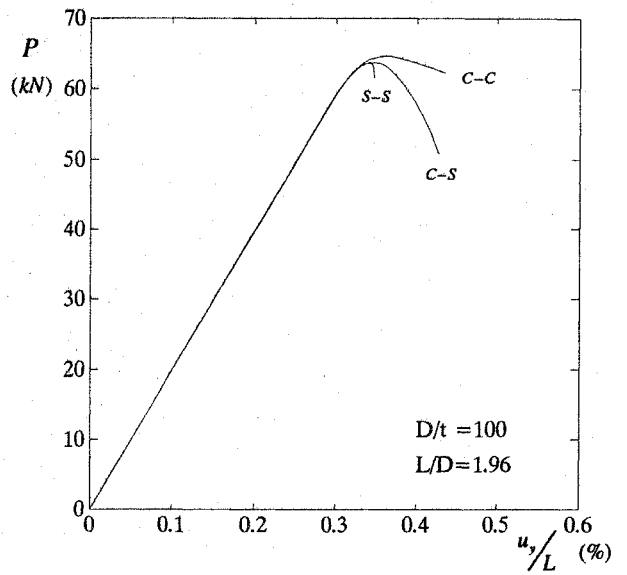

Fig. 6 Analytical load-displacement responses of circular cylindrical shells under axial compression with different boundary conditions.

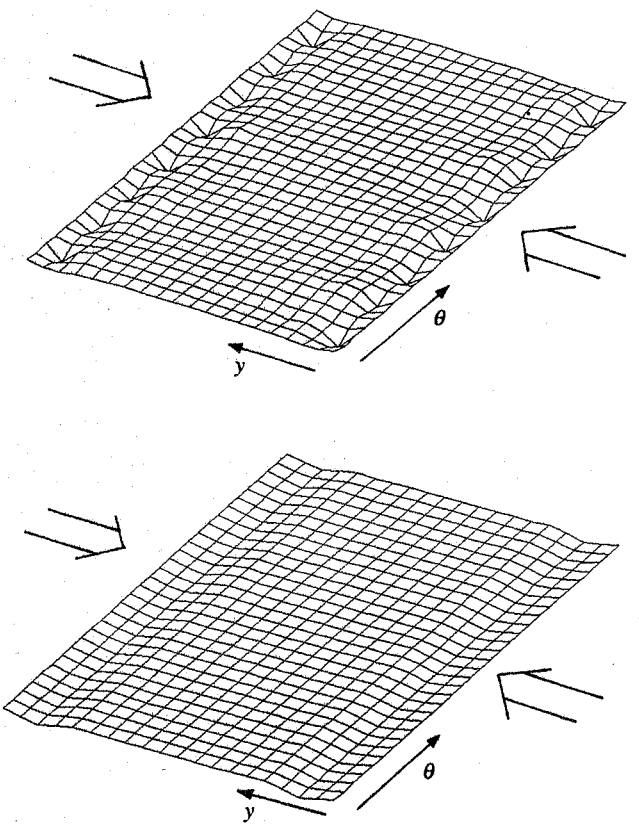

Fig. 7 Analytical buckling deformation of a circular cylindrical shell under axial compression with a) simply supported ends and b) clamped ends.

Axial Buckling Loads

Figure 8 shows the axial buckling loads of elastoplastic circular cylindrical shells with various lengths for ratios of diameter to thickness (D/t) of 100 and 133. The results show that the buckling loads alter slightly for ratio of length to diameter (L/D) up to 4 and the buckling behavior is termed as a "local" type. The analytical buckling loads of shells with $D/t = 133$ are much greater than experimental ones due to geometric imperfections of the testing specimens. The axial buckling loads of elastoplastic circular cylindrical shells with varied ratios of diameter to thickness are shown in Fig. 9. The buckling loads P were made dimensionless by

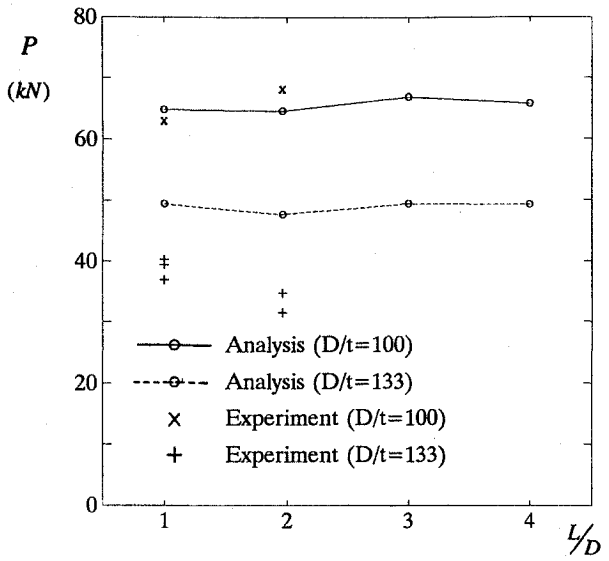

Fig. 8 Axial buckling loads of circular cylindrical shells for various ratios of length to diameter.

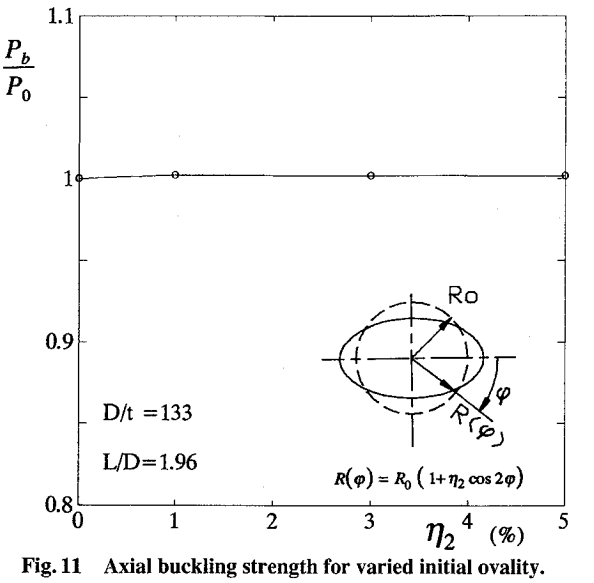

Fig. 11 Axial buckling strength for varied initial ovality.

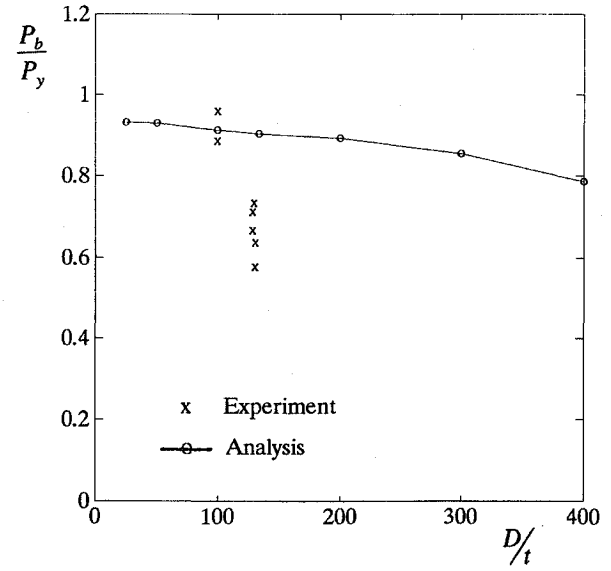

Fig. 9 Axial buckling loads of circular cylindrical shells for various ratios of diameter to thickness.

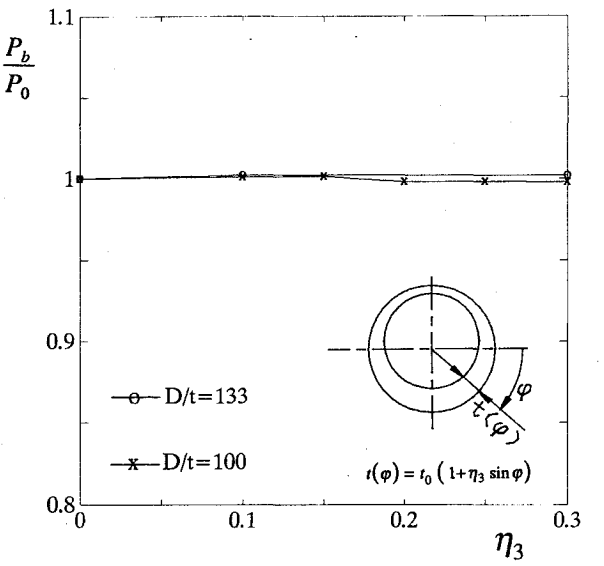

Fig. 12 Axial buckling strength for variations of initial thickness along the circumference of cross section.

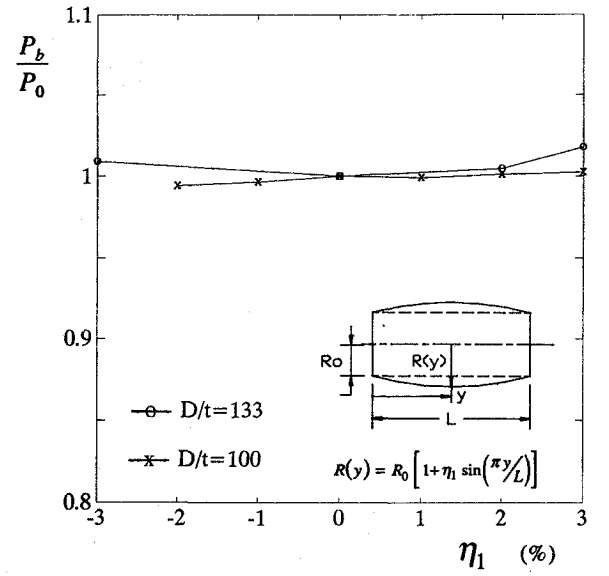

Fig. 10 Axial buckling strength for variations of initial radius along the axis of the circular cylindrical shell.

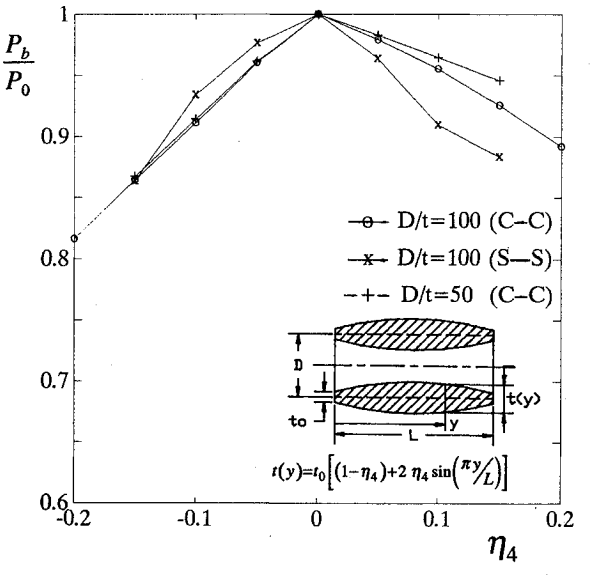

Fig. 13 Axial buckling strength for variations of initial thickness along the axis of the circular cylindrical shell.

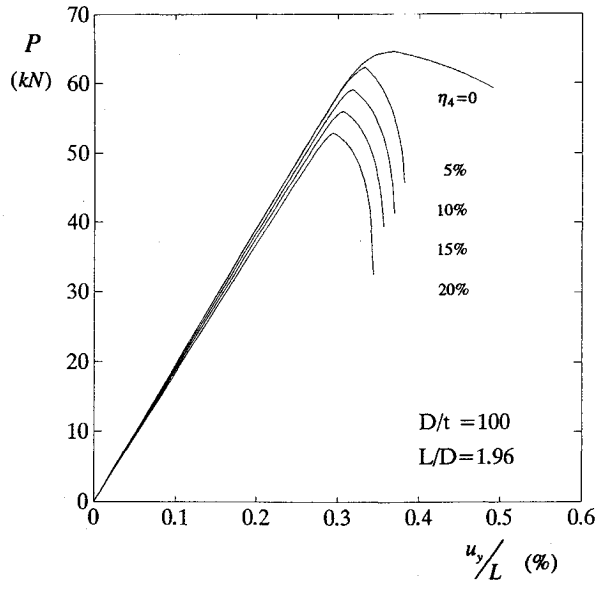

Fig. 14 Analytical load-displacement responses for variations of initial thickness along the axis of the circular cylindrical shell under axial compression.

$P_y = \pi D t \sigma_0$, and the dimensionless buckling loads decreased as the D/t ratio increasesd.

Initial Imperfections

Initial imperfections of four types and different boundary conditions were analyzed to find their influence on the elastoplastic buckling and postbuckling behavior of circular cylindrical shells under axial compression.

Radius Variations Along the Shell Axis

The geometry of a cylindrical shell with variations of initial radius along the shell axis is expressed as

$$R(y) = R_0[1 + \eta_1 \sin(\pi y/L)] \tag{21}$$

in which R_0 is the nominal radius, η_1 is an imperfection parameter, y is the axial coordinate, and L is the length of the shell. The initial geometry, Eq. (21), is referred to as out-of-straightness for axially symmetric imperfection.[5] The axial buckling loads P_b of circular cylindrical shells ($L/D = 1.96$) with $D/t = 100$ and 133 for various η_1 are shown in Fig. 10. The buckling loads were made dimensionless by dividing by the corresponding ones (P_0) with $\eta_1 = 0$. The axial elastoplastic buckling loads of circular cylindrical shells were only slightly influenced by η_1 values between -0.03 and 0.03.

Initial Ovality

Another initial radius imperfection considered is the ovality of the cross section of the circular cylindrical shell. The radius $R(\varphi)$ around the circumference is expressed as

$$R(\varphi) = R_0[1 + \eta_2 \cos 2\varphi] \tag{22}$$

in which η_2 is an imperfection parameter, and φ is the angular coordinate. The axial buckling loads P_b of circular cylindrical shells with $D = 2R_0 = 97$ mm, $D/t = 133$, and $L/D = 1.96$ are shown in Fig. 11. These buckling loads were made dimensionless by dividing by the corresponding one (P_0) with $\eta_2 = 0$. The axial elastoplastic buckling loads of circular cylindrical shells are almost the same for η_2 values less than 0.05. The assumed initial ovality, Eq. (22), was also used by Liu and Li[5] for cylindrical shells under external pressure combined with axial compression and by Tvergaard[26] for elliptical cylindrical shells compressed axially.

Thickness Variation Around the Circumference

The variation of thickness around the circumference of a circular cylindrical shell is expressed as

$$t(\varphi) = t_0[1 + \eta_3 \sin \varphi] \tag{23}$$

in which t_0 is the mean thickness, and η_3 is an imperfection parameter. The assumed thickness variation, Eq. (23), is similar to the geometric eccentricity mentioned in the paper by Liu and Li.[5] The axial buckling loads P_b of circular cylindrical shells ($L/D = 1.96$) with $D/t = 100$ and 133 for various η_3 values are shown in Fig. 12. These buckling loads were made dimensionless by dividing by the corresponding ones (P_0) with $\eta_3 = 0$. The axial elastoplastic buckling loads of circular cylindrical shells are shown to be almost the same for η_3 values less than 0.3.

Thickness Variation Along the Shell Axis

The variation of thickness along the axis of a circular cylindrical shell is expressed as

$$t(y) = t_0[(1-\eta_4) + 2\eta_4 \sin(\pi y/L)] \tag{24}$$

in which η_4 is an imperfection parameter. The axial buckling loads P_b of circular cylindrical shells ($L/D = 1.96$) with $D/t = 50$ and 100 for various η_4 values are shown in Fig. 13. These buckling loads were made dimensionless by dividing by the ones (P_0) with $\eta_4 = 0$. Figure 13 shows that the axial buckling loads were strongly influenced by η_4. The axial buckling loads decreased for both positive and negative η_4. The axial buckling loads of circular cylindrical shells with $D/t = 100$ were influenced more by η_4 than the ones with $D/t = 50$. The cases of both ends being clamped had greater buckling loads than the cases of both ends being simply supported. Figure 14 shows the analytical load-displacement responses of circular cylindrical shells with $D/t = 100$, $L/D = 1.96$, and both ends clamped for various positive η_4. Both the axial buckling loads and the axial displacement at buckling decreased as η_4 increased.

Conclusions

The elastoplastic buckling of circular cylindrical shells was investigated analytically and experimentally. For shells buckling in the plastic range, the elastoplastic analysis was adopted. For the cases considered, the following conclusions can be made.

1) The axial buckling load of the circular cylindrical shell is minimally influenced by the ratio of length to diameter in the range of $1 < L/D < 4$.

2) The ratios of elastoplastic buckling loads of circular cylindrical shells under axial compression to the corresponding yield loads decreased as the ratio of diameter to thickness (D/t) of shells increased, for circular cylindrical shells that buckle in the plastic range.

3) The axial buckling loads of circular cylindrical shells were slightly influenced by variations of the initial radius along the shell axis and by initial ovality for the assumed types of imperfection.

4) The elastoplastic buckling loads of circular cylindrical shells under axial compression were reduced by the thickness variations along the axis of the shell.

5) Boundary conditions had little influence on the buckling loads but caused different postbuckling behavior for circular cylindrical shells under axial compression.

References

[1]Ramsey, H., "Axisymmetric Buckling of a Cylindrical Elastic Cosserat Shell Under Axial Compression," *Quarterly Journal of Mechanics and Applied Mathematics*, Vol. 40, Pt. 3, 1987, pp. 415–429.

[2]Abu-Farsakh, G., and Lusher, J.K., "Buckling of Glass-Reinforced Plastic Cylindrical Shells Under Combined Axial Compression and External Pressure," *AIAA Journal*, Vol. 23, No. 12, 1985, pp. 1946–1951.

[3]Abu-Farsakh, G., "Experimental Buckling of GRP Cylindrical Shells," *Experimental Mechanics*, Vol. 27, No. 1, 1987, pp. 1–9.

[4]Hansen, J. S., "General Random Imperfections in the Buckling of Axially Loaded Cylindrical Shells," *AIAA Journal*, Vol. 15, No. 9, 1977, pp. 1250–1256.

[5]Liu, Z., and Li, D., "Numerical Analysis of Geometric Imperfection Influence on the Safety of Cylindrical Shell," *Computers & Structures*, Vol. 41, No. 3, 1991, pp. 547–551.

[6]Rotter, J. M., and Teng, J. G., "Elastic Stability of Cylindrical Shells with Weld Depressions," *Journal of Structural Engineering*, Vol. 115, No. 5, 1989, pp. 1244–1263.

[7]Rotter, J. M., and Zhang, Q., "Elastic Buckling of Imperfect Cylinders Containing Granular Solids," *Journal of Structural Engineering*, Vol. 116, No. 8, 1990, pp. 2253–2271.

[8]Krishnakumar, S., and Foster, C. G., "Axial Load Capacity of Cylindrical Shells with Local Geometric Defects," *Experimental Mechanics*, Vol. 31, No. 2, 1991, pp. 104–110.

[9]Krishnakumar, S., and Foster, C. G., "Multiple Geometric Defects: Their Effect on Stability of Cylindrical Shells," *Experimental Mechanics*, Vol. 31, No. 3, 1991, pp. 213–219.

[10]Foster, C. G., "Axial Compression Buckling of Conical and Cylindrical Shells," *Experimental Mechanics*, Vol. 27, No. 3, 1987, pp. 255–261.

[11]Bijlaard, P. P., "Theory and Test on the Plastic Stability of Plates and Shells," *Journal of the Aeronautical Sciences*, Vol. 16, Sept. 1949, pp. 529–541.

[12]Lee, L. H. N., "Inelastic Buckling of Initially Imperfect Cylindrical Shells Subject to Axial Compression," *Journal of the Aerospace Sciences*, Vol. 29, Jan. 1962, pp. 87–95.

[13]Batterman, S. C., "Plastic Buckling of Axially Compressed Cylindrical Shells," *AIAA Journal*, Vol. 3, No. 2, 1965, pp. 316–325.

[14]Sobel, L. H., and Newman, S. Z., "Plastic Buckling of Cylindrical Shells Under Axial Compression," *ASME Journal of Pressure Vessel Technology*, Vol. 102, Feb. 1980, pp. 40–44.

[15]Batterman, S. C., and Lee, L. H. N., "Effect of Modes on Plastic Buckling of Compressed Cylindrical Shells," *AIAA Journal*, Vol. 4, No. 12, 1966, pp. 2255–2257.

[16]Hutchinson, J. W., "Plastic Buckling," *Advances in Applied Mechanics*, edited by C. S. Yih, Vol. 14, Academic Press, New York, 1974, pp. 67–144.

[17]Gellin, S., "Effect of an Axisymmetric Imperfection on the Plastic Buckling of an Axially Compressed Cylindrical Shells," *ASME Journal of Applied Mechanics*, Vol. 46, March 1979, pp. 125–131.

[18]Yun, H., and Kyriakides, S., "On the Beam and Shell Modes of Buckling of Buried Pipelines," *Soil Dynamics and Earthquake Engineering*, Vol. 9, No. 4, 1990, pp. 179–193.

[19]Tvergaard, V., "Plastic Buckling of Axially Compressed Circular Cylindrical Shells," *Thin-Walled Structures*, Vol. 1, 1983, pp. 139–163.

[20]Tvergaard, V., "On the Transition from a Diamond Mode to an Axisymmetric Mode of Collapse in Cylindrical Shells," *International Journal of Solids and Structures*, Vol. 19, No. 10, 1983, pp. 845–856.

[21]Ramsey, H., "Localized Axisymmetric Plastic Buckling Deformation in Cylindrical Cosserat Shells Under Axial Compression," *International Journal of Plasticity*, Vol. 3, No. 3, 1987, pp. 193–210.

[22]Bathe, K. J., *Finite Element Procedures in Engineering Analysis*, Prentice-Hall, Englewood Cliffs, NJ, 1982.

[23]Yeh, M. K., and Wei, C. H., "Collapse Analysis of Elastoplastic Shells," *The Chinese Journal of Mechanics*, Vol. 6, No. 1, 1990, pp. 23–30.

[24]Ahmad, S., Irons, B. M., and Zienkiewicz, O. C., "Analysis of Thick and Thin Shell Structures by Curved Element," *International Journal for Numerical Methods in Engineering*, Vol. 2, 1970, pp. 419–451.

[25]Owen, D. R. J., and Figueiras, J. A., "Anisotropic Elastoplastic Finite Element Analysis of Thick and Thin Plates and Shells," *International Journal for Numerical Methods in Engineering*, Vol. 19, 1983, pp. 541–566.

[26]Tvergaard, V., "Buckling of Elastic-Plastic Oval Cylindrical Shells Under Axial Compression," *International Journal of Solids and Structures*, Vol. 12, 1976, pp. 683–691.